A Tunable, Simplified Model for Biological Latch Mediated Spring Actuated Systems

Andrés Cook,[1] Kaanthi Pandhigunta,[1] Mason A. Acevedo,[1] Adam Walker,[1] Rosalie L. Didcock,[1] Jackson T. Castro,[1] Declan O'Neill,[1] Raghav Acharya,[2] M. Saad Bhamla,[2] Philip S. L. Anderson[3] and Mark Ilton[1,*]

[1]Department of Physics, Harvey Mudd College, Claremont, CA 91711, USA, [2]School of Chemical and Biomolecular Engineering, Georgia Institute of Technology, Atlanta, Georgia 30318, USA and [3]Department of Evolution, Ecology, and Behavior, University of Illinois at Urbana-Champaign, Urbana, IL 61801, USA

*Corresponding author. milton@hmc.edu

Associate Editor: Name

FOR PUBLISHER ONLY Received on Date Month Year; revised on Date Month Year; accepted on Date Month Year

Abstract

We develop a model of latch-mediated spring actuated (LaMSA) systems relevant to comparative biomechanics and bioinspired design. The model contains five components: two motors (muscles), a spring, a latch, and a load mass. One motor loads the spring to store elastic energy and the second motor subsequently removes the latch, which releases the spring and causes movement of the load mass. We develop freely available software to accompany the model, which provides an extensible framework for simulating LaMSA systems. Output from the simulation includes information from the loading and release phases of motion, which can be used to calculate kinematic performance metrics that are important for biomechanical function. In parallel, we simulate a comparable, directly actuated system that uses the same motor and mass combinations as the LaMSA simulations. By rapidly iterating through biologically relevant input parameters to the model, simulated kinematic performance differences between LaMSA and directly actuated systems can be used to explore the evolutionary dynamics of biological LaMSA systems and uncover design principles for bioinspired LaMSA systems. As proof of principle of this concept, we compare a LaMSA simulation to a directly actuated simulation that includes either a Hill-type force-velocity trade-off or muscle activation dynamics, or both. For the biologically-relevant range of parameters explored, we find that the muscle force-velocity trade-off and muscle activation have similar effects on directly actuated performance. Including both of these dynamic muscle properties increases the accelerated mass range where a LaMSA system outperforms a directly actuated one.

Key words: biomechanics, biological springs, computational modeling

Introduction

A diverse array of organisms use stored elastic energy to drive rapid movements. These organisms use motors, springs, and latches to perform a latch mediated spring actuated (LaMSA) motion, and remarkably, they can use this mechanism to outperform current engineering design for repeatable motion at small size-scales [Longo et al., 2019]. Models have been developed to understand the extreme biomechanics of latch-mediated spring actuated organisms. Organism-specific models, including both continuum mechanics-based models [Liu et al., 2017, Bolmin et al., 2019, Berg et al., 2019, Cooper et al., 2018, Hamlet et al., 2020, Wan and Hao, 2020, Larabee et al., 2018, Tadayon et al., 2018, Li et al., 2020] and physical modeling with biomimetic devices [Cox et al., 2014, Liu et al., 2017, Li et al., 2020, Singh et al., 2020, Büsse et al., 2021, Xu and Bhamla, 2019], have been used to test hypotheses about the movement of specific organisms (Table 1 summarizes examples of recent work).

In contrast to organism-specific models, 'simple models' with reduced complexity [Anderson et al., 2020] are primarily used for making inter-species comparisons, and for testing

Modeling Approach	Biomechanical System	Reference
Continuum mechanics		
beam bending model	click beetle latch	Bolmin et al. [2019]
fluid dynamics	bladderwort trap suction feeding	Berg et al. [2019]
	Ruellia ciliatiflora seed aerodynamics	Cooper et al. [2018]
	nematocyst discharge	Hamlet et al. [2020]
finite elements	locust jump	Wan and Hao [2020]
	dracula ant mandible strike	Larabee et al. [2018]
	mantis shrimp strike	Tadayon et al. [2018]
	Oxalis sp. seed ejection	Li et al. [2020]
Physical modeling		
	Oxalis sp. seed ejection	Li et al. [2020]
	bladderwort trap suction feeding	Singh et al. [2020]
	dragonfly larvae strike	Büsse et al. [2021]
	Spirostomum ambiguum contraction	Xu and Bhamla [2019]

Table 1. Recent examples (since 2018) of modeling latch-mediated spring actuated organisms, which includes both mathematical and physical approaches. For a review of earlier work see ref. [Ilton et al., 2018].

scaling relationships and the sensitivity of kinematic performance to different characteristics of the organism. These simple models can also have broad applicability and enable the rapid testing of ideas [Anderson et al., 2020], and typically include muscle motors, springs, masses, and other mechanical linkages. In recent work, these models have been applied to jumping organisms [Olberding et al., 2019, Jarur et al., 2019, Davranoglou et al., 2019, Zhang et al., 2020, Niechciał et al., 2019, Hong et al., 2020, Mo et al., 2020, Sutton et al., 2019] and augmented human movements [Sutrisno and Braun, 2019, 2020]. General models have also been used to test hypotheses about the scaling and effectiveness of biological spring mechanisms [Galantis and Woledge, 2003, Ilton et al., 2018, Abbott et al., 2019, Sutton et al., 2019, Divi et al., 2020]. These types of models have similarities to template models – simple biomechanical models that demonstrate a particular mechanical behavior [Full and Koditschek, 1999].

Previous work used a simplified mathematical model to illustrate trade-offs between the components of a general LaMSA system [Ilton et al., 2018]. The components of a LaMSA system (the latch, spring, loading motor, and load mass) were modeled as a simplified mechanical system and given material, geometric, and dynamic properties; however, the properties of the system components were limited to motors and springs with linear properties, specific latch shapes, frictionless interactions between components, and a fixed unlatching velocity.

Here, we develop a LaMSA Template Model with accompanying software. Our model here includes a more general framework for defining LaMSA components, such that previous LaMSA modeling efforts [Galantis and Woledge, 2003, Ilton et al., 2018, Sutton et al., 2019, Divi et al., 2020] are all particular cases of this new model. This broader approach allows the model to be tuned to a specific organism, group of organisms, or a biological scaling relationship to explore questions in comparative biomechanics and LaMSA system design. Our approach also includes non-linear and time-dependent properties of the spring material during unloading. Additionally, we provide a generalized treatment of the latch that includes friction, allows for different latch shapes, and includes an unlatching motor that drives the latch removal of the system, similar to the one recently hypothesized to occur in some biological systems [Büsse et al., 2021].

Finally, as an example of this LaMSA model's utility, we use the model to explore how dynamic muscle properties affect the power output of both a LaMSA system and a system where the muscle is used to directly actuate movement. Two important dynamic aspects of muscle are a force-velocity trade-off (the muscle exerts less force at higher velocities) and an activation rate (it takes some time for the muscle to reach its maximum force) [Rosario et al., 2016]. Previous work has been focused on how muscle force-velocity trade-offs limit power output for a directly actuated system [Galantis and Woledge, 2003, Ilton et al., 2018]. This force-velocity trade-off is a principal reason LaMSA systems can outperform comparable muscle-driven ones at small load mass; however, it is unclear how significant this force-velocity effect is compared to the activation dynamics of muscle. Here we directly compare the effect of the muscle force-velocity trade-off to the effect of muscle activation. Using the LaMSA Template Model with inputs guided by biologically-relevant sizes and masses, we find that the muscle force-velocity trade-off and activation dynamics cause a similar reduction in directly actuated kinematics. Combining the two effects, the mass range where a LaMSA system outperforms a directly actuated one increases by a factor of ≈ 5 times compared to systems where only one of the two time dependent motor properties is included.

Methods

LaMSA Template Model

In our model, the motion of a LaMSA system is comprised of three distinct phases: loading, unlatching, and spring actuation. In the loading phase (Fig. 1A, first panel), a loading motor (e.g. muscle) deforms a spring starting from the spring's stress-free equilibrium length. We make the simplifying assumption that the loading occurs slowly enough to approximate it as a quasi-static motor contraction – i.e. the loading follows the isometric force-length curve in the case of a muscle motor. Loading is complete when the loading motor force pulling down (in the $-y$ direction) matches the spring force pulling up. After the loading

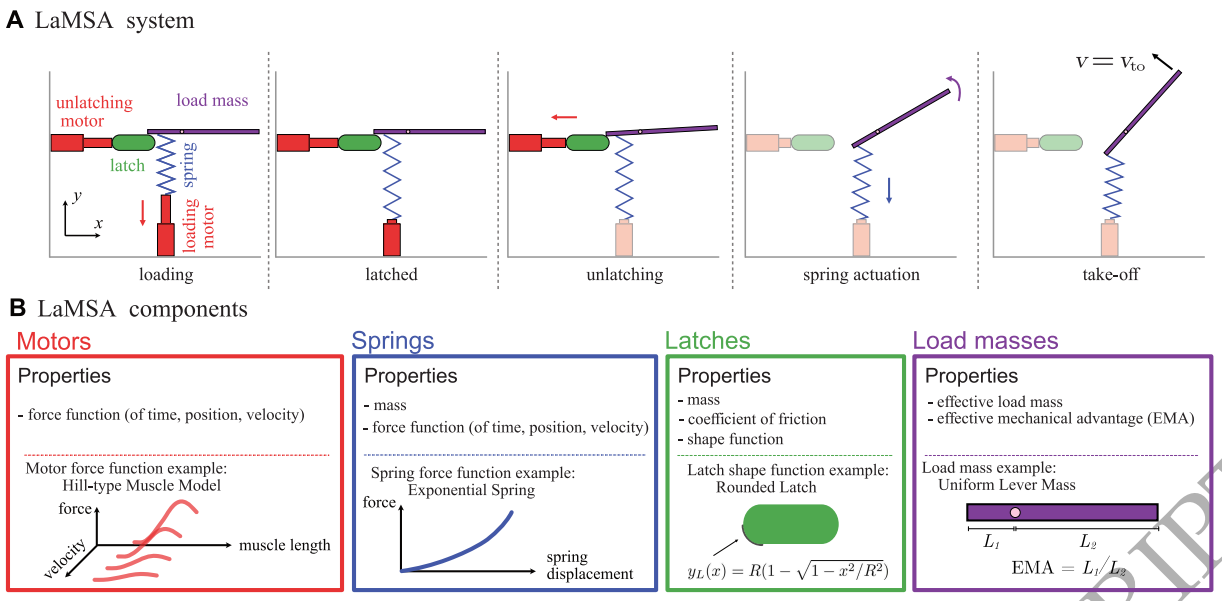

Fig. 1: Schematic description of the LaMSA Template Model with a loading motor, spring, latch, unlatching motor, and load mass. **A** The sequence of important events during the movement of a LaMSA system, which includes three delineated phases of motion in the model: loading, unlatching, and spring actuation. **B** The properties of the components used in the LaMSA Template Model, and an example of each component that is explored in this work (see Table A1 in Appendix A for the specific example functions and parameters used in this manuscript).

phase, the loading motor remains at a fixed displacement and the spring is held in place by a latch (Fig. 1A, second panel). The second phase of motion, the unlatching phase (Fig. 1A, third panel), begins with the activation of an unlatching motor that pulls the latch out of the way. During the unlatching phase the load mass and latch undergo a complex interaction. The interaction between the load mass and latch is modeled as a frictional contact between two rigid bodies, and the unlatching phase ends when there is no longer any contact between the load mass and latch. Once the contact breaks, the load mass is actuated solely by the spring, which undergoes a rapid unloading (Fig. 1A, fourth panel). Spring actuation continues until the spring returns to its equilibrium length where it no longer applies a force to the load mass, which corresponds to the "take-off" of the load mass (Fig. 1A, fifth panel). In the model, we assume that the latch shape is sufficiently smooth that after the latch disengages, it does not re-engage at a later time. This assumption enables the clear delineation of the unlatching and spring actuation phases.

The dynamics of a LaMSA system depends on its components and the interaction between them. In our model, these components are classified into motors, springs, latches, and load masses (Fig. 1B). Each motor is constrained to move along a single coordinate axis in the model (the loading motor moves along the y axis; the latch and unlatching motor move along the x axis). We develop our model with the aim to give general properties to each component. The motors and springs in the LaMSA system are characterized by their force output. The loading motor force (F_{lm}), the unlatching motor force (F_{um}), and spring force (F_{sp}) are all assumed to be functions of time, displacement, and velocity. Latches are given a shape function $y_L(x)$ that describes the geometry of the latch. The shape function relates horizontal motion of the latch (in the x direction) to vertical displacements of the load (in the y direction). For example, the rounded latch used in this work, which has circular edges of radius R, has a shape function shown in Fig. 1B. The shape function describes the shape of the latch where it contacts the load mass. The derivatives of this shape function with respect to x determine the latch slope function $y_L\prime(x) = \frac{dy_L}{dx}$ and latch concavity $y_L\prime\prime(x) = \frac{d^2y_L}{dx^2}$. The functions describing shapes and forces are taken as inputs into the model to allow for hypothesis testing of non-linear properties. In addition, the mass of the system can be distributed in the spring mass, latch mass, and load mass. With these definitions, we lay out the mathematical description of the model according to its three phases of motion.

LaMSA Template Model: Loading Phase

In the loading phase, the loading motor slowly applies a force causing a displacement of the spring. The final displacement of the spring at the end of the loading phase, y_0, is the displacement in which the loading motor force and spring force are equal and opposite, namely

$$F_{\mathrm{lm}}(t = \infty, y_0, \dot{y} = 0) = -F_{\mathrm{sp}}(t = \infty, y_0, \dot{y} = 0), \quad (1)$$

where $\dot{y}$ is the velocity in the y direction. The condition that $t = \infty$ and $\dot{y} = 0$ corresponds to a slow, quasi-static loading of the spring. The loaded displacement, y_0, depends on how the force-displacement properties of the loading motor and spring interact.

LaMSA Template Model: Unlatching Phase

The unlatching phase starts with the activation of the unlatching motor at time $t = 0$. The spring starts with an initial

displacement y_0 and velocity $\dot{y} = 0$, while the latch has an initial horizontal position $x = 0$ and velocity $\dot{x} = v_0$. By analyzing the spring force acting on the load mass, the unlatching motor force pulling on the latch, and the contact force between the load mass and latch, we derive that the differential equation for the acceleration of the latch, $\ddot{x}$, during the unlatching phase of motion

$$\ddot{x} = \frac{(F_{\text{um}}+F_{\text{sp}}y'_L-m_{\text{eff}}y'_Ly''_L\dot{x}^2)+\mu_k(F_{\text{um}}y'_L-F_{\text{sp}}+m_{\text{eff}}y''_L\dot{x}^2)}{(m_L+m_{\text{eff}}(y'_L)^2)-\mu_k(m_{\text{eff}}y'_L-m_Ly'_L)}, \quad (2)$$

where μ_k is the coefficient of friction between the latch and load, and m_L is the mass of the latch. The term m_{eff} in Eq. (2) is the overall effective mass for the mass-spring system, with $m_{\text{eff}} = m_{\text{load}} + m_s/3$ [Ilton et al., 2018], where m_s is the spring mass and m_{load} is the effective load mass that depends on load mass and its effective mechanical advantage (EMA). A full derivation of Eq. (2) is presented in Appendix B for a system undergoing small angular displacements. For a LaMSA system undergoing large angular displacements during rotational motion, the effective mass and mapping onto Eq. (2) is provided in Appendix C. From the dynamics and shape of the latch, the acceleration of the load mass during the unlatching phase is given by the chain rule,

$$\ddot{y} = y''_L\dot{x}^2 + y'_L\ddot{x}. \quad (3)$$

To determine the end of the unlatching phase, we solve for the magnitude of the normal component of the contact force between the load mass and latch,

$$F_N = \frac{-m_LF_{\text{sp}}+m_Lm_{\text{eff}}y''_L\dot{x}^2+m_{\text{eff}}y'_LF_{\text{um}}}{m_{\text{eff}}y'_L\mu_k-m_{\text{eff}}(y'_L)^2-m_L\mu_ky'_L-m_L}\sqrt{1+(y'_L)^2}, \quad (4)$$

and require that this magnitude be non-negative during the unlatching phase to ensure there is still contact between the load mass and latch. Therefore, we solve for when $F_N = 0$ to determine the unlatching duration t_L, which marks the end of the unlatching phase and the beginning of the spring actuation phase of motion.

LaMSA Template Model: Spring Actuation Phase

After unlatching, the load mass undergoes a purely spring-driven motion given by

$$\ddot{y} = \frac{F_{\text{sp}}}{m_{\text{eff}}}, \quad (5)$$

where the spring force can depend on position, velocity, and time. The initial conditions for this phase are given by the ending condition from the unlatching phase: for the spring actuation phase, the initial position of the load mass is $y(t = t_L)$ and its initial velocity is $\dot{y}(t = t_L)$. The spring actuation phase ends when the spring stops pushing on the load mass, i.e. when $F_{\text{sp}} = 0$.

Direct Actuation Model

The direct actuation model uses the loading motor of the LaMSA system to directly drive the load mass. To ensure the motor in the directly actuated model is being used in a comparable way to the LaMSA model, the mass is accelerated by the motor using a motor contraction. Therefore, the equation of motion for the load mass is given directly by the force applied by the motor as it contacts,

$$\ddot{y} = \frac{F_{\text{lm}}}{m_{\text{eff}}}, \quad (6)$$

where the loading motor force can depend on position, velocity and time. The initial condition for the directly actuated system is that the motor and load mass are initially at rest, with the motor at its undisplaced initial length. Take-off occurs when the load mass reaches its maximum velocity and $F_{\text{lm}} = 0$.

LaMSA and Direct Actuation Software Implementation

The LaMSA and direct actuation models were implemented in MATLAB. This software implementation is freely redistributable and available at https://posmlab.github.io [Didcock et al., 2020]. The software allows a user to select a LaMSA system from a library of components (motors, springs, latches, and load masses), set parameters for each component, and run a simulation to determine the dynamics of that system (as both a LaMSA system and a directly actuated system). The software can be used to iterate over the LaMSA system component parameters (e.g. spring stiffness) and rapidly generate the dynamics for variety of LaMSA systems.

Model Input Parameters

The input parameters to the model were chosen based on the accelerated mass, characteristic velocities, and typical accelerations of the larger biological LaMSA systems listed in the supplementary materials of ref. [Ilton et al., 2018]. To explore the role of the dynamic properties of muscle, we used a Hill-type muscle motor based on ref. [Rosario et al., 2016], which is one of the default components included in the LaMSA Template Model software. A muscle activation rate of $200\,\text{s}^{-1}$ was chosen as a typical rate based on the force generation delay of small animals reported in ref. [More and Donelan, 2018]. The full list of parameters used in this work are reported in Table A1.

Results and Discussion

Using the components and parameters in Table A1, the output from a single simulation generated using the software is shown in Fig. 2. The software output includes information about the loading phase, and the dynamics of the latch and load mass during the unlatching and spring actuation phases. For the load mass dynamics, the simulation generates the position $y(t)$, velocity $\dot{y}(t)$, and forces acting on the load mass. From the position and velocity of the load mass, commonly used metrics for kinematic performance in biomechanics (e.g. maximum acceleration and maximum power [Longo et al., 2019]) are calculated. The maximum load mass acceleration ($\max|\ddot{y}(t)|$, calculated from the numerical derivative of $\dot{y}(t)$) and maximum power delivered to the load mass ($P_{\max} = \max|m\ddot{y}(t)\dot{y}(t)|$) depend on the input parameters to the model, and the freely redistributable software enables a rapid iteration over a range of input parameters.

For a motor directly actuating a load mass, the maximum power output depends on accelerated mass, with an upper bound set by the dynamic properties of the motor (Fig. 3, red curves). Driving the mass with a motor that has only a force-velocity trade-off (setting $r_{\text{act}} = \infty$ and $v_{\max} = 5\,\text{m/s}$ in the model) has a similar effect to a motor that only has activation

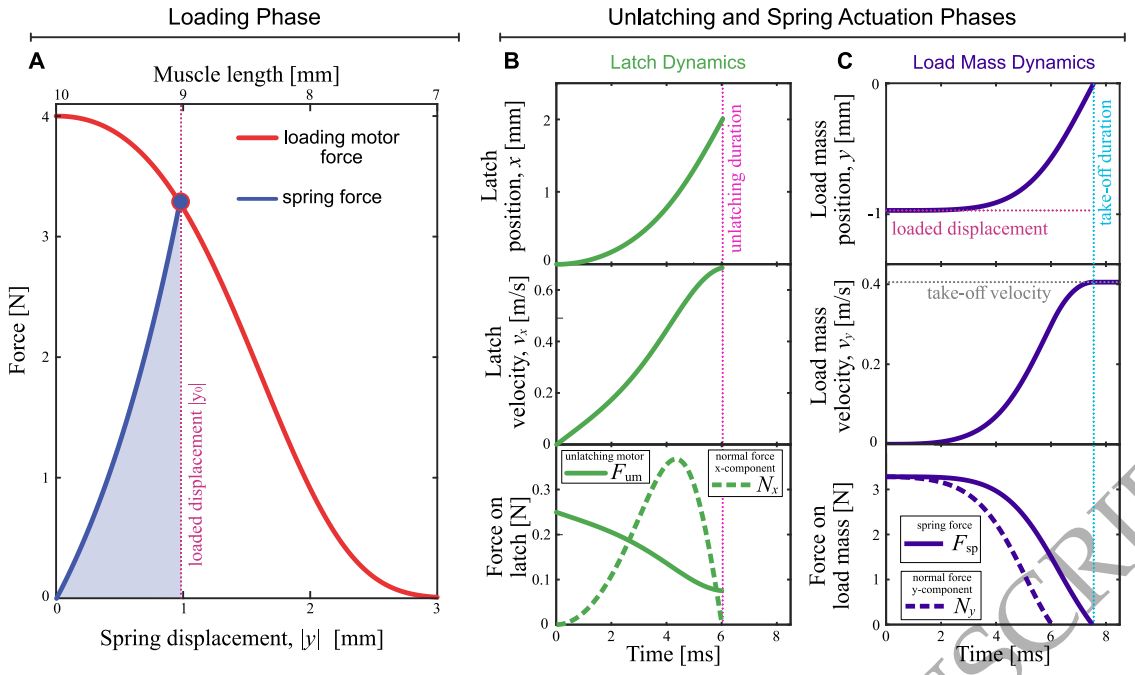

Fig. 2: Example output from the model using the components and the biological LaMSA parameters listed in Table A1. **A** The force-length curve for a Hill-type muscle motor loading a tendon-like exponential spring. The LaMSA system loads up to a spring displacement $y_{\max}$ calculated by equating the loading motor and spring forces. **B-C** The dynamics during the unlatching and spring actuation phases for the latch (panel B) and load mass (panel C). The end of the unlatching phase is marked by the pink vertical dotted line showing the unlatching duration ($t_L \approx 6\,\text{ms}$), which occurs when the normal force N between the latch and load mass goes to zero (dashed curves in B-C). After unlatching, the load mass is actuated solely by the spring up until take-off duration ($t_{\text{to}} \approx 7.5\,\text{ms}$) when the spring force goes to zero, and the load mass reaches its take-off velocity ($v_{\text{to}} \approx 0.4\,\text{m/s}$).

dynamics (setting $r_{\text{act}} = 200\,\text{s}^{-1}$ and $v_{\max} = \infty$ in the model). Both motors reach an upper bound on their maximum power output when driving small masses (Fig. 3, dashed and dotted red curves). Therefore, even in the absence of a force-velocity trade-off, motors with slow activation rates still have performance limitations when driving small masses. Including both the effects of force-velocity and activation in the motor, as projectile mass is decreased the maximum power output of a directly actuated movement not only saturates to a maximum value, but further decreases for the smallest masses (Fig. 3, solid red curve).

In contrast to the directly actuated systems, the LaMSA system is insensitive to the force-velocity trade-offs and activation dynamics of the loading motor. Varying the loading motor in the LaMSA system using the same three conditions as the directly actuated one (activation dynamics only, F-v trade-off only, F-v trade-off and activation dynamics), the maximum output for those three LaMSA systems is identical (Fig. 3, solid blue curve). The independence of the LaMSA system on the dynamic properties of the loading motor is a result of the slow, quasi-static loading assumption made in the model. This assumption is justified for biological LaMSA systems like mantis shrimp where typical loading rates are orders of magnitude slower than the rate of elastic energy release [Patek, 2019], but the loading motor dynamic properties can be important when considering simultaneous loading and release of a series elastic system [Galantis and Woledge, 2003].

The power output of comparable LaMSA and directly actuated systems have a mass dependent transition that is affected by the dynamic properties of the motor. Comparing the three different motor conditions in Fig. 3, the crossovers between the power output of the directly actuated and LaMSA systems is shifted to a larger mass (by a factor of ≈ 5 times) when both the force-velocity and activation dynamics of the motor are included in the simulation. This result suggests that in systems where there is a development and transition of a LaMSA mechanism (e.g. in some species of mantis shrimp [Harrison et al., 2021]), care should be given to both muscle force-velocity and activation dynamics when modeling the transition from LaMSA to directly actuated movement.

Although the results of Fig. 3 were generated using general, biologically-relevant parameter values for LaMSA systems, a more specific biological system could be used to guide further inquiry into the relative importance of force-velocity versus muscle activation dynamics. For example, although here we assumed a fixed value of EMA = 1, the mechanical advantage in both muscle-driven and spring-driven systems can significantly alter dynamics [Richards and Clemente, 2012, Olberding et al., 2019]. Decreasing the EMA in the current model shifts the drop-off in muscle-driven performance to smaller masses. In addition, for most biologically-relevant

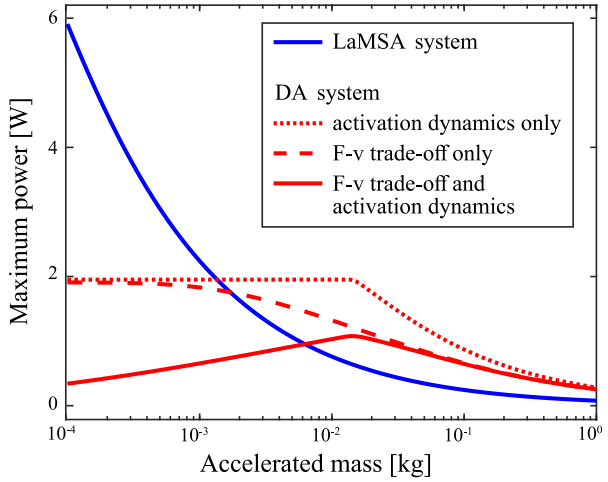

Fig. 3: Both a motor's activation rate and its force-velocity trade-off affect its maximum power output when it directly actuates a projectile. Compared to a using a motor in a LaMSA system (blue solid curve), the maximum power output of a directly actuated system (red curves) is worse for smaller masses. A motor that has both a force-velocity and activation limitation (solid red curve) has a significantly reduced performance at low masses compared to one with only a force-velocity trade-off (dashed red curve) or only an activation rate limitation (dotted red curve). The intersection between the LaMSA and directly actuated curve shifts to a higher mass when both dynamic effects of the motor are included.

systems maximum muscle force typically increases as system size increases. With a specific system in mind, appropriate scaling [Rospars and Meyer-Vernet, 2016] and fair comparisons [Ilton et al., 2019] could be made across size-scales for both motor-driven and elastically-driven systems.

Beyond this proof of principle example, the LaMSA Template Model and freely redistributable software provides an extensible platform for exploring biological LaMSA systems. Although this model was formulated generally to encompass a broad range of LaMSA systems, the model can be tuned to specific biological systems because of the flexibility in how system components are defined. The relevant range of input parameters and any interdependence between them can be informed by observed biological data and scaling. For example, depending on the system, the characteristic lengths of the system (i.e. muscle lengths, latch radius, spring length) could be constrained in the model to follow an isometric scaling. The software allows the user to enforce mathematical couplings between the different input parameters to the model, which can be used make inter-species comparisons and to investigate to what extent kinematic performance changes over the course of development for a given species.

Flexible component definitions also enables new components to be created that address specific biological questions. For example, Deban *et al.* performed a comparative analysis of tongue projection across salamander species which actuate their tongue projection with a LaMSA mechanism or by direct muscle actuation [Deban et al., 2020]. The LaMSA projection mechanism can not only lead to higher kinematic performance, but is also robust to temperature variations [Deban et al., 2020]. To explore this system with the LaMSA model presented here, new components can be created in the software that introduce a temperature-dependent motor and spring. Adding these components would yield a theoretical prediction of the relative sensitivity of the tongue projection performance to temperature for the two groups of salamanders. Comparing this prediction to the observed kinematics could be used to inform the modeling of how biological motors and springs depend on temperature. As an additional example, Acharya *et al.* built on the general LamSA framework here to include non-linear soft frictional latches to understand the ultrafast motion of human finger snaps [Acharya et al., 2021].

Finally, the model and software presented here can offer insights into how the interrelationships between input parameters and performance may influence the evolution of these biological systems via the concept of mechanical sensitivity. Mechanical sensitivity refers to the idea that variation between parts of a multi-part system are not necessarily equal in relation to their influence on the output of the system [Koehl, 1996, Anderson and Patek, 2015]. Applied to a LaMSA system, we might hypothesize that variation in the spring would result in a larger variation in maximum power than variation in the latch mass. If so, that could mean that the latch mass has more freedom to evolve without altering performance. Such patterns have been identified in both mantis shrimp and fish [Anderson and Patek, 2015, Hu et al., 2017] and have been shown to influence rates of morphological evolution [Muñoz et al., 2017, 2018, Muñoz, 2019]. The model presented here offers an opportunity to quantitatively map how shifts in input parameters affect multiple performance metrics simultaneously, allowing for a comprehensive analysis of mechanical sensitivity.

Conclusion

The LaMSA Template Model and software presented here balances modeling principles of simplicity and extensibility. Simplicity is provided by making explicit assumptions about how the components are connected in the model, and extensibility is achieved though flexibility of defining the individual components. With these principles, the model enables the rapid testing of ideas by simulating kinematic output across the varying model parameters. This model also opens possible new directions for future work by providing a framework for others to build upon. Case studies using the model will inform best practices for tuning the model to explore a specific biological system. Exploring biological and bioinspired LaMSA systems with this model will require input from members of comparative biomechanics community through the use of the software (available at https://posmlab.github.io [Didcock et al., 2020]), requesting new features, and actively contributing to software development.

Author Contributions

AC and MI designed the research; all authors contributed to the model development; AC, KP, MAA, AW, RLD, JTC, DO, RA, and MI wrote the software; AC and MI wrote a first draft of the manuscript; all authors revised and edited the manuscript.

Acknowledgments

This material is based upon work supported by the National Science Foundation under Grant No. 2019371. We thank the Harvey Mudd College Physics Summer Research Fund and the N. Sprague III Experiential Learning Fund for financial support. MSB acknowledges funding support from NSF Career 1941933 and NIH R35GM142588. The authors thank S.N. Patek and Justin Jorge for stimulating discussions and helpful suggestions on this work.

References

E. M. Abbott, T. Nezwek, D. Schmitt, and G. S. Sawicki. Hurry up and get out of the way! exploring the limits of muscle-based latch systems for power amplification. *Integrative and Comparative Biology*, 59(6):1546–1558, 2019. ISSN 15577023. doi: 10.1093/icb/icz141.

R. Acharya, E. J. Challita, M. Ilton, and M. Saad Bhamla. The ultrafast snap of a finger is mediated by skin friction. *Journal of the Royal Society Interface*, 18(184):20210672, 2021.

P. S. Anderson and S. N. Patek. Mechanical sensitivity reveals evolutionary dynamics of mechanical systems. *Proceedings of the Royal Society B: Biological Sciences*, 282(1804), 2015. ISSN 14712954. doi: 10.1098/rspb.2014.3088.

P. S. L. Anderson, M. D. Rivera, and A. V. Suarez. "Simple" biomechanical model for ants reveals how correlated evolution among body segments minimizes variation in center of mass as heads get larger. *Integrative and Comparative Biology*, icaa027, may 2020. ISSN 1540-7063. doi: 10.1093/icb/icaa027. https://academic.oup.com/icb/advance-article/doi/10.1093/icb/icaa027/5835282.

O. Berg, K. Singh, M. R. Hall, M. J. Schwaner, and U. K. Müller. Thermodynamics of the bladderwort feeding strike - Suction power from elastic energy storage. *Integrative and Comparative Biology*, 59(6):1597–1608, 2019. ISSN 15577023. doi: 10.1093/icb/icz144.

O. Bolmin, L. Wei, A. M. Hazel, A. C. Dunn, A. Wissa, and M. Alleyne. Latching of the click beetle (Coleoptera: Elateridae) thoracic hinge enabled by the morphology and mechanics of conformal structures. *Journal of Experimental Biology*, 222 (12), 2019. ISSN 00220949. doi: 10.1242/jeb.196683.

S. Büsse, A. Koehnsen, H. Rajabi, and S. N. Gorb. A controllable dual-catapult system inspired by the biomechanics of the dragonfly larvae's predatory strike. *Science Robotics*, 6(50), 2021.

E. S. Cooper, M. A. Mosher, C. M. Cross, and D. L. Whitaker. Gyroscopic stabilization minimizes drag on Ruellia ciliatiflora seeds. *Journal of the Royal Society Interface*, 15(140), 2018. ISSN 17425662. doi: 10.1098/rsif.2017.0901.

S. M. Cox, D. Schmidt, Y. Modarres-Sadeghi, and S. N. Patek. A physical model of the extreme mantis shrimp strike: Kinematics and cavitation of Ninjabot. *Bioinspiration and Biomimetics*, 9(1), 2014. ISSN 17483182. doi: 10.1088/1748-3182/9/1/016014.

L. R. Davranoglou, A. Cicirello, G. K. Taylor, and B. Mortimer. Planthopper bugs use a fast, cyclic elastic recoil mechanism for effective vibrational communication at small body size. *PLoS Biology*, 17(3):1–17, 2019. ISSN 15457885. doi: 10.1371/journal.pbio.3000155.

S. M. Deban, J. A. Scales, S. V. Bloom, C. M. Easterling, M. K. O'Donnell, and J. P. Olberding. Evolution of a high-performance and functionally robust musculoskeletal system in salamanders. *Proceedings of the National Academy of Sciences of the United States of America*, 117(19):10445–10454, 2020. ISSN 10916490. doi: 10.1073/pnas.1921807117.

R. L. Didcock, K. Pandhigunta, M. Ilton, J. T. Castro, M. A. Acevedo, A. Cook, and A. Walker. MATLAB LaMSA Model, Aug 2020. URL `https://doi.org/10.5281/zenodo.3978584`.

S. Divi, X. Ma, M. Ilton, R. S. Pierre, B. Eslami, S. N. Patek, and S. Bergbreiter. Latch-based control of energy output in spring actuated systems. *Journal of the Royal Society Interface*, 17(168):20200070, 2020. URL `https://doi.org/10.1098/rsif.2020.0070`.

R. J. Full and D. E. Koditschek. Templates and anchors: Neuromechanical hypotheses of legged locomotion on land. *Journal of experimental biology*, 202(23):3325–3332, 1999.

A. Galantis and R. C. Woledge. The theoretical limits to the power output of a muscle-tendon complex with inertial and gravitational loads. *Proceedings of the Royal Society B: Biological Sciences*, 270(1523):1493–1498, 2003. ISSN 14712970. doi: 10.1098/rspb.2003.2403.

C. Hamlet, W. Strychalski, and L. Miller. Fluid dynamics of ballistic strategies in nematocyst firing. *Fluids*, 5(1):1–18, 2020. ISSN 23115521. doi: 10.3390/fluids5010020.

J. S. Harrison, M. L. Porter, M. J. McHenry, H. E. Robinson, and S. Patek. Scaling and development of elastic mechanisms: the tiny strikes of larval mantis shrimp. *Journal of Experimental Biology*, 224(8):jeb235465, 2021.

C. Hong, D. Tang, Q. Quan, Z. Cao, and Z. Deng. A combined series-elastic actuator & parallel-elastic leg no-latch bio-inspired jumping robot. *Mechanism and Machine Theory*, 149:103814, 2020. ISSN 0094114X. doi: 10.1016/j.mechmachtheory.2020.103814. URL `https://doi.org/10.1016/j.mechmachtheory.2020.103814`.

Y. Hu, N. Nelson-Maney, and P. S. Anderson. Common evolutionary trends underlie the four-bar linkage systems of sunfish and mantis shrimp. *Evolution*, 71(5):1397–1405, 2017. ISSN 15585646. doi: 10.1111/evo.13208.

M. Ilton, M. Saad Bhamla, X. Ma, S. M. Cox, L. L. Fitchett, Y. Kim, J. sung Koh, D. Krishnamurthy, C. Y. Kuo, F. Z. Temel, A. J. Crosby, M. Prakash, G. P. Sutton, R. J. Wood, E. Azizi, S. Bergbreiter, and S. N. Patek. The principles of cascading power limits in small, fast biological and engineered systems. *Science*, 360(6387), 2018. ISSN 10959203. doi: 10.1126/science.aao1082.

M. Ilton, S. M. Cox, T. Egelmeers, G. P. Sutton, S. N. Patek, and A. J. Crosby. The effect of size-scale on the kinematics of elastic energy release. *Soft Matter*, 15(46):9579–9586, 2019. ISSN 17446848. doi: 10.1039/c9sm00870e.

M. C. Jarur, J. Dumais, and S. Rica. Limiting speed for jumping. *Comptes Rendus - Mecanique*, 347(4):305–317, 2019. ISSN 16310721. doi: 10.1016/j.crme.2019.03.005. URL `https://doi.org/10.1016/j.crme.2019.03.005`.

M. A. Koehl. When does morphology matter? *Annual Review of Ecology and Systematics*, 27:501–542, 1996. ISSN 00664162. doi: 10.1146/annurev.ecolsys.27.1.501.

F. J. Larabee, A. A. Smith, and A. V. Suarez. Snap-jaw morphology is specialized for high-speed power amplification in the Dracula ant, Mystrium camillae. *Royal Society Open Science*, 5(12), 2018. ISSN 20545703. doi: 10.1098/rsos.181447.

S. Li, Y. Zhang, and J. Liu. Seed ejection mechanism in an Oxalis species. *Scientific Reports*, 10(1):1–9, 2020. ISSN 20452322. doi: 10.1038/s41598-020-65885-2.

F. Liu, R. L. Chavez, S. N. Patek, A. Pringle, J. J. Feng, and C. H. Chen. Asymmetric drop coalescence launches fungal ballistospores with directionality. *Journal of the Royal Society Interface*, 14(132), 2017. ISSN 17425662. doi: 10.1098/rsif.2017.0083.

S. J. Longo, S. M. Cox, E. Azizi, M. Ilton, J. P. Olberding, R. St Pierre, and S. N. Patek. Beyond power amplification: Latch-mediated spring actuation is an emerging framework for the study of diverse elastic systems. *Journal of Experimental Biology*, 222(15):1–10, 2019. ISSN 00220949. doi: 10.1242/jeb.197889.

X. Mo, D. Romano, M. Milazzo, G. Benelli, W. Ge, and C. Stefanini. Impact of Different Developmental Instars on Locusta migratoria Jumping Performance. *Applied Bionics and Biomechanics*, 2020:27–29, 2020. ISSN 17542103. doi: 10.1155/2020/2797486.

J. A. Monroy, K. L. Powers, C. M. Pace, T. Uyeno, and K. C. Nishikawa. Effects of activation on the elastic properties of intact soleus muscles with a deletion in titin. *Journal of Experimental Biology*, 220(5):828–836, 2017. ISSN 00220949. doi: 10.1242/jeb.139717.

H. L. More and J. M. Donelan. Scaling of sensorimotor delays in terrestrial mammals. *Proceedings of the Royal Society B*, 285(1885):20180613, 2018.

M. M. Muñoz. The Evolutionary Dynamics of Mechanically Complex Systems. *Integrative and Comparative Biology*, 59 (3):705–715, 2019. ISSN 15577023. doi: 10.1093/icb/icz077.

M. M. Muñoz, P. S. Anderson, and S. N. Patek. Mechanical sensitivity and the dynamics of evolutionary rate shifts in biomechanical systems. *Proceedings of the Royal Society B: Biological Sciences*, 284(1847), 2017. ISSN 14712954. doi: 10.1098/rspb.2016.2325.

M. M. Muñoz, Y. Hu, P. S. Anderson, and S. N. Patek. Strong biomechanical relationships bias the tempo and mode of morphological evolution. *eLife*, 7:1–18, 2018. ISSN 2050084X. doi: 10.7554/eLife.37621.

M. Niechciał, D. Rybarczyk, and J. Buśkiewicz. Modelling the monopedal robot. *IOP Conference Series: Materials Science and Engineering*, 710(1), 2019. ISSN 1757899X. doi: 10.1088/1757-899X/710/1/012030.

J. P. Olberding, S. M. Deban, M. V. Rosario, and E. Azizi. Modeling the determinants of mechanical advantage during jumping: Consequences for spring- And muscle-driven movement. *Integrative and Comparative Biology*, 59(6):1515–1524, 2019. ISSN 15577023. doi: 10.1093/icb/icz139.

S. N. Patek. The Power of Mantis Shrimp Strikes: Interdisciplinary Impacts of an Extreme Cascade of Energy Release. *Integrative and Comparative Biology*, 59(6):1573–1585, 07 2019. ISSN 1540-7063. doi: 10.1093/icb/icz127. URL `https://doi.org/10.1093/icb/icz127`.

C. T. Richards and C. J. Clemente. A bio-robotic platform for integrating internal and external mechanics during muscle-powered swimming. *Bioinspiration & biomimetics*, 7(1): 016010, 2012.

M. V. Rosario, G. P. Sutton, S. N. Patek, and G. S. Sawicki. Muscle-spring dynamics in time-limited, elastic movements. *Proceedings of the Royal Society B: Biological Sciences*, 283 (1838), 2016. ISSN 14712954. doi: 10.1098/rspb.2016.1561.

J. P. Rospars and N. Meyer-Vernet. Force per cross-sectional area from molecules to muscles: A general property of biological motors. *Royal Society Open Science*, 3(7), 2016. ISSN 20545703. doi: 10.1098/rsos.160313.

K. Singh, R. C. Reyes, G. C. Campa, M. D. Brown, F. Hidalgo, O. Berg, and U. K. Müller. Suction flows generated by the carnivorous bladderwort utricularia—comparing experiments with mechanical and mathematical models. *Fluids*, 5(1):17–22, 2020. ISSN 23115521. doi: 10.3390/fluids5010033.

A. Sutrisno and D. J. Braun. Enhancing Mobility with Quasi-Passive Variable Stiffness Exoskeletons. *IEEE Transactions on Neural Systems and Rehabilitation Engineering*, 27(3): 487–496, 2019. ISSN 15344320. doi: 10.1109/TNSRE.2019.2899753.

A. Sutrisno and D. J. Braun. How to run 50% faster without external energy. *Science Advances*, 6(13):1–11, 2020. ISSN 23752548. doi: 10.1126/sciadv.aay1950.

G. P. Sutton, E. Mendoza, E. Azizi, S. J. Longo, J. P. Olberding, M. Ilton, and S. N. Patek. Why do large animals never actuate their jumps with latch-mediated springs? because they can jump higher without them. *Integrative and Comparative Biology*, 59(6):1609–1618, 2019. ISSN 15577023. doi: 10.1093/icb/icz145.

M. Tadayon, S. Amini, Z. Wang, and A. Miserez. Biomechanical Design of the Mantis Shrimp Saddle: A Biomineralized Spring Used for Rapid Raptorial Strikes. *iScience*, 8:271–282, 2018. ISSN 25890042. doi: 10.1016/j.isci.2018.08.022. URL `https://doi.org/10.1016/j.isci.2018.08.022`.

C. Wan and Z. Hao. Natural arrangement of micro-strips reduces shear strain in the locust cuticle during power amplification. *Journal of Biomechanics*, 107:109842, 2020. ISSN 18732380. doi: 10.1016/j.jbiomech.2020.109842. URL `https://doi.org/10.1016/j.jbiomech.2020.109842`.

L. X. Xu and M. S. Bhamla. Biophysical mechanism of ultra-fast helical twisting contraction in the giant unicellular ciliate Spirostomum ambiguum. *bioRxiv*, pages 1–10, 2019. doi: 10.1101/854836v1. URL `https://doi.org/10.1101/854836`.

Z. Zhang, B. Chang, J. Zhao, Q. Yang, and X. Liu. Design, Optimization, and Experiment on a Bioinspired Jumping Robot with a Six-Bar Leg Mechanism Based on Jumping Stability. *Mathematical Problems in Engineering*, 2020, 2020. ISSN 15635147. doi: 10.1155/2020/3507203.

Appendices

Appendix A: Table of Parameters Used

Loading Motor

Force Function: (ref. [Rosario et al., 2016])

$F_{\mathrm{lm}}(t, y, \dot{y}) = F_{\max} \exp\left(-\left|((\frac{L_i - y}{L_o})^b - 1)/s\right|^a\right) \left(\frac{1 - \dot{y}/v_{\max}}{1 + 4\dot{y}/v_{\max}}\right) \min(r_{\mathrm{act}}\, t, 1)$

Loading Motor parameters used in this work:

$F_{\max} = 20\,\mathrm{N}$ $v_{\max} = \{5, \infty\}\ \mathrm{m/s}$ $L_o = L_i = 10\,\mathrm{mm}$

$a = 2.08$ $b = -2.89$ $s = -0.75$ $r_{\mathrm{act}} = \{200, \infty\}\ \mathrm{s}^{-1}$

Spring

Force Function: (ref. [Monroy et al., 2017])

$$F_{\mathrm{sp}}(t, y, \dot{y}) = \begin{cases} l_c\, k_0 e^{-y/l_c} - 1, & \text{for } F_{\mathrm{sp}} < F_{\mathrm{s,max}} \\ F_{\mathrm{s,max}}, & \text{otherwise} \end{cases}$$

Spring parameters used in this work:

$l_c = 10\,\mathrm{mm}$ $k_0 = 2\,\mathrm{kN/m}$ $F_{\mathrm{sp,max}} = 20\,\mathrm{N}$ $m_s = 20\,\mathrm{mg}$

Latch

Shape Function: (ref. [Ilton et al., 2018])

$y_L(x) = R(1 - \sqrt{1 - x^2/R^2})$

Default Latch Parameters Used:

$R = 0.2\,\mathrm{mm}$ $m_L = 3\,\mathrm{g}$ $\mu_k = 0$ $v_0 = 0$

Unlatching Motor

Force Function: (ref. [Ilton et al., 2018])

$$F_{\mathrm{um}}(t, x, \dot{x}) = \begin{cases} F_{\max}(1 - \frac{\dot{x}}{v_{\max}}), & \text{for } 0 \le x \le d \\ 0, & \text{otherwise} \end{cases}$$

Unlatching Motor parameters used in this work:

$F_{\max} = 0.25\,\mathrm{N}$ $v_{\max} = 1\,\mathrm{m/s}$ $d = 5\,\mathrm{mm}$

Load Mass

Load Mass parameters used in this work:

$m_{\mathrm{load}} = 0.1 - 100\,\mathrm{kg}$

$\mathrm{EMA} = 1$

Table A1. Mathematical description of the LaMSA components and default parameter values used in this work. The parameters were selected based on the range of characteristic forces, lengths, and velocities for biological LaMSA systems [Ilton et al., 2018, More and Donelan, 2018].

Appendix B: Derivation of the Model

To simplify the model derivation, we will first reduce our general model that can include rotation down to a one-dimensional representation. For an applied force F at one end of a rotating rod with a fixed pivot:

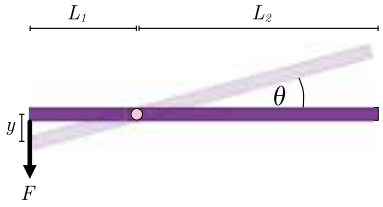

The dynamics of the system is given by relating the applied torque about the pivot to the angular acceleration of the rod,

$$FL_1 = I\ddot{\theta}, \tag{7}$$

where I is the moment of inertia of the load mass about the fixed pivot point, which for a uniform rod of mass m is given by

$$I = \frac{1}{12}m(L_1 + L_2)^2 + m\left(\frac{L_2 - L_1}{2}\right)^2. \tag{8}$$

If the angular displacement is small (see Appendix C: Model for Large Angular Displacements for a derivation of the reduced model for large angular displacements), then the linear displacement of the point where force is applied $y \approx L_1\theta$, can be substituted into the equation of motion to give,

$$F = \frac{I}{L_1^2}\ddot{y}, \tag{9}$$

which for a uniform load mass simplifies to

$$F = m_{\text{load}}\ddot{y}, \tag{10}$$

with the effective load mass

$$m_{\text{load}} = m\left(\frac{(1 + \frac{1}{\text{EMA}})^2}{12} + \frac{(1 - \frac{1}{\text{EMA}})^2}{4}\right). \tag{11}$$

In other words, the rotational system reduces down to one-dimensional dynamics of the point of where force is applied, but with an effective load mass that takes into account the effective mechanical advantage of the system.

With that simplification, we consider a reduced complexity one dimensional Latch Mediated Spring Actuated (LaMSA) system:

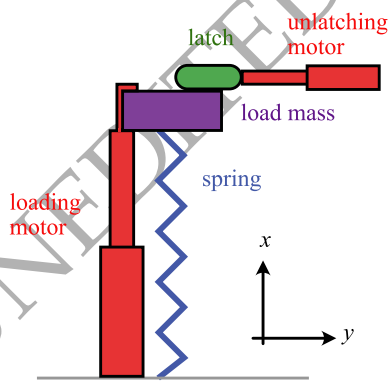

Our goal is to derive a single ordinary differential equation describing x(t) of the latch while it is in contact with the load mass.

Setting Up the Problem

Let us approximate the load mass and latch as point masses and draw isolation diagrams. In this model, we will consider the latch to have some shape that governs the unlatching process. Therefore, we have some function $y_L(x)$ that determines the curve of the latch.

Variables:

$m_{\text{eff}} = m_{\text{load}} + \frac{m_{\text{spring}}}{3}$: the effective mass of the load mass and spring mass combined
F_{sp} : force exerted by the spring on the load mass
μ_k : coefficient of friction between the load mass and the latch
F_N : normal force
F_f : force of friction between latch and load mass

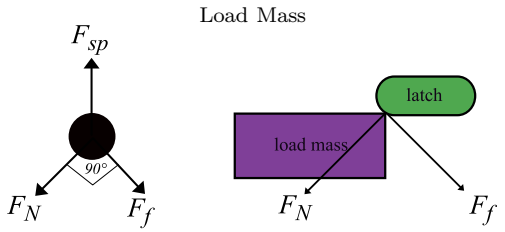

θ : The angle between the normal force vector and the vertical

Among these variables, we'll consider the following to be given:
F_{sp}, μ_k

With names for our variables, we can write Newton's second law to get the following:

$$\begin{aligned}\sum F_y = m_{\text{eff}}\ddot{y} =& F_{\text{sp}} - F_{N_y} - F_{f_y} \\ m_{\text{eff}}\ddot{y} =& F_{\text{sp}} - F_N \cos\theta - \mu_k F_N \cos(90 - \theta) \\ m_{\text{eff}}\ddot{y} =& F_{\text{sp}} - F_N \cos\theta - \mu_k F_N \sin\theta\end{aligned}$$

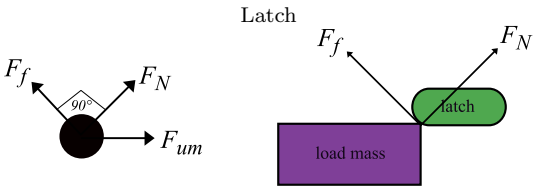

Variables:
m_L : mass of the latch
F_{um} : force of the unlatching motor pulling the latch away
F_N : Normal force from load mass on latch
F_f : Friction force from load mass on latch
$y_L(x)$: function describing the latch geometry

Known Values:

m_L : mass of the latch
F_{um} : force of the unlatching motor pulling the latch away
$y_L(x)$: function describing the latch geometry

We get the following equations from Newton's 2nd Law:

$$\begin{aligned}\sum F_x = m_L(\ddot{x}) =& F_{\text{um}} + F_{N_x} - F_{f_x} \\ m_L(\ddot{x}) =& F_{\text{um}} + F_N \sin\theta - \mu_k F_N \sin(90-\theta) \\ m_L(\ddot{x}) =& F_{\text{um}} + F_N \sin\theta - \mu_k F_N \cos\theta\end{aligned}$$

Rewriting Unknowns in Terms of Other Variables
We will use these replacements later in the derivation.

Rewriting $\ddot{y}$ - Our goal is to get a differential equation for $\ddot{x}$, but we will end up with $\ddot{y}$ in our equations. So, we can use the following to rewrite $\ddot{y}$ in terms of $\ddot{x}$ and the latch curve:

$$\begin{aligned}\ddot{y} =& \frac{d}{dt}\left(\frac{dy}{dt}\right) \\ =& \frac{d}{dt}\left(\frac{dy}{dx}\cdot\frac{dx}{dt}\right) \\ =& \frac{d}{dt}(y'_L\cdot\dot{x}) \\ =& y''_L\cdot\dot{x}^2 + y'_L\cdot\ddot{x}\end{aligned}$$

Rewriting $\tan\theta$ - We will need to replace $\tan\theta$ later in the derivation.

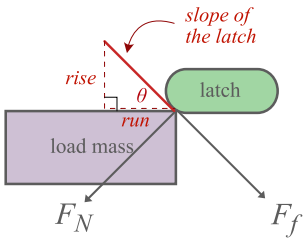

Because the latch geometry is described by the function y_L, the slope of the latch is described by the derivative y'_L.

$$\begin{aligned}y'_L &= \frac{rise}{run} \\ \tan\theta &= \frac{rise}{run} \\ \tan\theta &= y'_L\end{aligned}$$

Solving for $\ddot{x}$

Solving for F_N in each equation- Recall that we obtained the following two equations from applying Newton's 2nd Law to both :

$$m_{\text{eff}}(\ddot{y}) = F_{\text{sp}} - F_N\cos\theta - \mu_k F_N\sin\theta$$
$$m_L(\ddot{x}) = F_{\text{um}} + F_N\sin\theta - \mu_k F_N\cos\theta$$

Let us replace $\ddot{y}$ with the expression we obtained in the previous section. Now we have:

$$m_{\text{eff}}(y_L''\cdot\dot{x}^2 + y_L'\cdot\ddot{x}) = F_{\text{sp}} - F_N\cos\theta - \mu_k F_N\sin\theta \tag{12}$$
$$m_L(\ddot{x}) = F_{\text{um}} + F_N\sin\theta - \mu_k F_N\cos\theta \tag{13}$$

The only element that is not known is F_N. Let us eliminate it by solving for F_N in both equations. Solving for F_N in Eq. (12) gives us:

$$F_N = \frac{F_{\text{sp}} - m_{\text{eff}}(y_L''\cdot\dot{x}^2 + y_L'\cdot\ddot{x})}{\cos\theta + \mu_k\sin\theta}$$

Solving for F_N in Eq. (13) gives us:

$$F_N = \frac{m_L\ddot{x} - F_{\text{um}}}{\sin\theta - \mu_k\cos\theta}$$

Expressing F_N without using $\ddot{x}$ - While it is our ultimate goal to solve for $\ddot{x}$, a side goal that is useful for determining the end of the unlatching phase is obtaining an expression for F_N that does not include $\ddot{x}$.

We can achieve this by taking Eqs. (12) and (13) from the previous section, isolating $\ddot{x}$ in each, and setting them equal to each other.

Rearranging Eq. (12):

$$\begin{aligned} m_{\text{eff}}(y_L''\cdot\dot{x}^2 + y_L'\cdot\ddot{x}) &= F_{\text{sp}} - F_N\cos\theta - \mu_k F_N\sin\theta \\ m_{\text{eff}}y_L'\ddot{x} &= F_{\text{sp}} - F_N\cos\theta - \mu_k F_N\sin\theta - m_{\text{eff}}y_L''\dot{x}^2 \\ \ddot{x} &= \frac{F_{\text{sp}} - F_N\cos\theta - \mu_k F_N\sin\theta - m_{eff}y_L''\dot{x}^2}{m_{eff}y_L'} \end{aligned}$$

Rearranging Eq. (13):

$$\begin{aligned} m_L(\ddot{x}) &= F_{\text{um}} + F_N\sin\theta - \mu_k F_N\cos\theta \\ \ddot{x} &= \frac{F_{\text{um}} + F_N\sin\theta - \mu_k F_N\cos\theta}{m_L} \end{aligned}$$

Setting these equal to each other, isolating F_N:

$$\frac{F_{\text{sp}} - F_N\cos\theta - \mu_k F_N\sin\theta - m_{eff}y_L''\dot{x}^2}{m_{eff}y_L'} = \frac{F_{\text{um}} + F_N\sin\theta - \mu_k F_N\cos\theta}{m_L}$$
$$m_L(F_{\text{sp}} - F_N\cos\theta - \mu_k F_N\sin\theta - m_{eff}y_L''\dot{x}^2) = m_{eff}y_L'(F_{\text{um}} + F_N\sin\theta - \mu_k F_N\cos\theta)$$

$$\begin{aligned} -F_N m_L\cos\theta - F_N m_L\mu_k\sin\theta - F_N m_{eff}y_L'\sin\theta + F_N m_{eff}y_L'\mu_k\cos\theta = \\ m_L m_{eff}y_L''\dot{x}^2 - m_L F_{\text{sp}} \\ + m_{eff}y_L'F_{\text{um}} \\ F_N(m_{eff}y_L'\mu_k\cos\theta - m_{eff}y_L'\sin\theta - m_L\mu_k\sin\theta - m_L\cos\theta) = \\ m_L m_{eff}y_L''\dot{x}^2 - m_L F_{\text{sp}} \\ + m_{eff}y_L'F_{\text{um}} \end{aligned}$$

$$F_N = \frac{m_L m_{eff}y_L''\dot{x}^2 - m_L F_{\text{sp}} + m_{eff}y_L'F_{\text{um}}}{m_{eff}y_L'\mu_k\cos\theta - m_{eff}y_L'\sin\theta - m_L\mu_k\sin\theta - m_L\cos\theta}$$

It's somewhat inconvenient to have θ in this expression, so we can make the following substitutions based on the geometry of our problem:

$$\sin\theta = \frac{y'_L}{\sqrt{1+(y_L\prime)^2}} \qquad \cos\theta = \frac{1}{\sqrt{1+(y_L\prime)^2}}$$

Plugging these in:

$$F_N = \frac{m_L m_{eff} y''_L \dot{x}^2 - m_L F_{\text{sp}} + m_{eff} y'_L F_{\text{um}}}{m_{eff} y'_L \mu_k - m_{eff}(y'_L)^2 - m_L \mu_k y'_L - m_L}\sqrt{1+(y'_L)^2}$$

Great! Now that we have this, we'll resume with our other goal, of solving for $\ddot{x}$.

Solving for $\ddot{x}$ - With two expressions for F_N in Eqs. (12) and (13), we can set them equal to each other to solve for $\ddot{x}$:

$$\frac{F_{\text{sp}} - m_{\text{eff}}(y''_L \cdot \dot{x}^2 + y'_L \cdot \ddot{x})}{\cos\theta + \mu_k \sin\theta} = \frac{m_L \ddot{x} - F_{\text{um}}}{\sin\theta - \mu_k \cos\theta}$$

Cross-multiply to get:

$$(\sin\theta - \mu_k\cos\theta)(F_{\text{sp}} - m_{\text{eff}}(y''_L \cdot \dot{x}^2 + y'_L \cdot \ddot{x}) = (\cos\theta + \mu_k \sin\theta)(m_L\ddot{x} - F_{\text{um}})$$

Expanding:

$$F_{\text{sp}}\sin\theta - m_{\text{eff}}\sin\theta(y''_L \cdot \dot{x}^2 + y'_L \cdot \ddot{x}) - F_{\text{sp}}\mu_k\cos\theta + m_{\text{eff}}\mu_k\cos\theta(y''_L \cdot \dot{x}^2 + y'_L \cdot \ddot{x}) =$$
$$m_L\ddot{x}\cos\theta - F_{\text{um}}\cos\theta + m_L\mu_k\ddot{x}\sin\theta - F_{\text{um}}\mu_k\sin\theta$$

Divide both sides by $\cos\theta$:

$$F_{\text{sp}}\frac{\sin\theta}{\cos\theta}^{\tan\theta} - m_{\text{eff}}\frac{\sin\theta}{\cos\theta}^{\tan\theta}(y''_L \cdot \dot{x}^2 + y'_L \cdot \ddot{x}) - F_{\text{sp}}\mu_k\frac{\cos\theta}{\cos\theta} + m_{\text{eff}}\mu_k\frac{\cos\theta}{\cos\theta}(y''_L \cdot \dot{x}^2 + y'_L \cdot \ddot{x})$$
$$= m_L\ddot{x}\frac{\cos\theta}{\cos\theta} - F_{\text{um}}\frac{\cos\theta}{\cos\theta} + m_L\mu_k\ddot{x}\frac{\sin\theta}{\cos\theta}^{\tan\theta} - F_{\text{um}}\mu_k\frac{\sin\theta}{\cos\theta}^{\tan\theta}$$
$$F_{\text{sp}}\tan\theta - m_{\text{eff}}\tan\theta(y''_L \cdot \dot{x}^2 + y'_L \cdot \ddot{x}) - F_{\text{sp}}\mu_k + m_{\text{eff}}\mu_k(y''_L \cdot \dot{x}^2 + y'_L \cdot \ddot{x})$$
$$= m_L\ddot{x} - F_{\text{um}} + m_L\mu_k\ddot{x}\tan\theta - F_{\text{um}}\mu_k\tan\theta$$

We can replace $\tan\theta$ with y'_L:

$$F_{\text{sp}}y'_L - m_{\text{eff}}y'_L(y''_L \cdot \dot{x}^2 + y'_L \cdot \ddot{x}) - F_{\text{sp}}\mu_k + m_{\text{eff}}\mu_k(y''_L \cdot \dot{x}^2 + y'_L \cdot \ddot{x})$$
$$= m_L\ddot{x} - F_{\text{um}} + m_L\mu_k\ddot{x}y'_L - F_{\text{um}}\mu_k y'_L$$

If we expand the equation, move all terms that contain $\ddot{x}$ and $\dot{x}^2$ to one side, and factor out $\ddot{x}$ and $\dot{x}^2$, we get:

$$\ddot{x}(m_{\text{eff}}\mu_k y'_L - m_{\text{eff}}(y'_L)^2 - m_L - m_L\mu_k y'_L) + \dot{x}^2(m_{\text{eff}}\mu_k y''_L - m_{\text{eff}}y'_L y''_L)$$
$$= -F_{\text{um}} - F_{\text{um}}\mu_k y'_L - F_{\text{sp}}y'_L + F_{\text{sp}}\mu_k$$

Now, let us solve for $\ddot{x}$ and regroup some terms to arrive at the final result:

$$\boxed{\ddot{x} = \frac{(F_{\text{um}} + F_{\text{sp}}y'_L) + \mu_k(F_{\text{um}}y'_L - F_{\text{sp}}) - \dot{x}^2(m_{\text{eff}}y'_L y''_L - m_{\text{eff}}\mu_k y''_L)}{(m_L + m_{\text{eff}}(y'_L)^2) - \mu_k(m_{\text{eff}}y'_L - m_L y'_L)}}$$

And if there is no friction such that $\mu_k = 0$:

$$\boxed{\ddot{x} = \frac{(F_{\text{um}} + F_{\text{sp}}y'_L) - \dot{x}^2(m_{\text{eff}}y'_L y''_L)}{m_L + m_{\text{eff}}(y'_L)^2}}$$

Appendix C: Model for Large Angular Displacements

To model large amplitude rotational motion, we can no longer assume $F_{spring} = m_{proj} \cdot \ddot{y}$ as we do for the case of linear (or small amplitude rotational) motion. Instead, there is a changing mechanical advantage as a function of the angle between the spring and the lever (pictured below) that complicates the dynamics of the system.

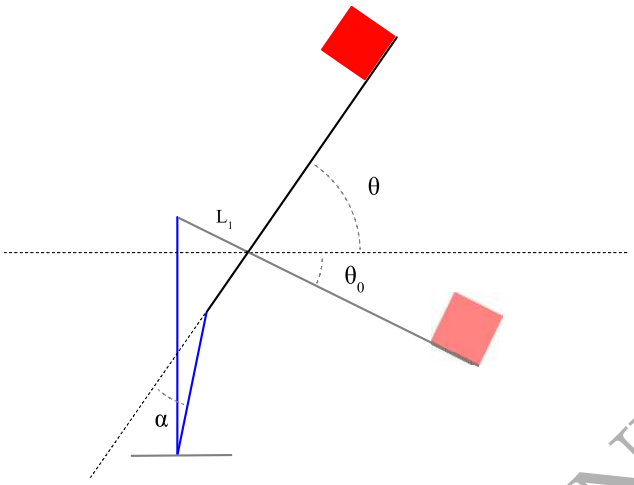

However, if we derive expressions for effective spring force and projectile mass F_{eff} and m_{eff} as functions of the displacement of the spring, we can use these expressions in our linear model to accurately describe rotational motion. In the following section, we derive these expressions.

We begin by writing Newton's second law for rotational motion:

$$F \cdot \sin(\alpha) \cdot L_1 = I\ddot{\theta}. \tag{14}$$

Our end goal is to write this as

$$F_{\text{eff}} = m_{\text{eff}} \cdot \ddot{y}$$

where y is the displacement of the spring.

First, we will write $\ddot{\theta}$ in terms of $\ddot{y}$. There is a complex exact relationship between y and θ that an interested reader can calculate using the law of cosines a few times, but it is very well approximated by $y = L_1 \cdot \sin(\theta)$. Using this, we find

$$\begin{aligned} y &= L_1 \cdot \sin(\theta) \\ \dot{y} &= L_1 \cdot \cos(\theta) \cdot \dot{\theta} \\ \ddot{y} &= -L_1 \cdot \sin(\theta) \cdot \dot{\theta}^2 + L_1 \cdot \cos(\theta) \cdot \ddot{\theta} \end{aligned}$$

.

Rearranging these equations, we find

$$\ddot{\theta} = \frac{1}{L_1 \cos(\theta)}\ddot{y} + \frac{\sin(\theta)}{L_1^2 \cos^3(\theta)}\dot{y}^2 \tag{15}$$

Now, if we substitute equation 15 into equation 14, we have

$$F \cdot \sin(\alpha) = \frac{I}{L_1^2}\left(\frac{1}{\cos(\theta)}\ddot{y} + \frac{\sin(\theta)}{L_1\cos^3(\theta)}\dot{y}^2\right) \tag{16}$$

Next, we find $\frac{I}{L_1^2}$. Using the parallel axis theorem, we find the moment of inertia of the lever (a rod with uniformly distributed mass m) and projectile (a point mass M) about the axis of rotation will be

$$I = M(L_2)^2 + \frac{1}{12}m(L_1+L_2)^2 + m\left(\frac{L_2-L_1}{2}\right)^2$$

.

Dividing by L_1^2 and substituting the effective mechanical advantage $EMA = \frac{L_1}{L_2}$, we have found an intermediate mass quantity m_{int} such that

$$m_{\text{int}} = \frac{I}{L_1^2} = \left(\frac{M}{EMA^2} + \frac{m}{12}\left(\left(1+\frac{1}{EMA}\right)^2 + 3\left(\frac{1}{EMA}-1\right)^2\right)\right)$$

and we can rewrite equation 16 as

$$F \cdot \sin(\alpha) = m_{\text{int}} \cdot \left(\frac{1}{\cos(\theta)}\ddot{y} + \frac{\sin(\theta)}{L_1\cos^3(\theta)}\dot{y}^2\right)$$

or

$$F\sin(\alpha) - m_{\text{int}}\frac{\sin(\theta)}{L_1\cos^3(\theta)}\dot{y}^2 = \frac{m_{\text{int}}}{\cos(\theta)}\cdot\ddot{y} \tag{17}$$

Equation 17 is in the desired form, so we can now extract

$$F_{\text{eff}} = F\sin(\alpha) - m_{\text{int}}\frac{\sin(\theta)}{L_1\cos^3(\theta)}\dot{y}^2$$

and

$$m_{\text{eff}} = \frac{m_{\text{int}}}{\cos(\theta)}.$$